Contribution from the Science Center, Rockwell International, Thousand Oaks, California 91360, and from the Rocketdyne Division, Rockwell International, Canoga Park, California 91304

# Electron Spin Resonance Study of $O_2^+$ Salts. Influence of Crystal Field Effects and Relaxation

IRA B. GOLDBERG,* KARL O. CHRISTE, and RICHARD D. WILSON

*Received June 14, 1974* AIC40379C

Electron spin resonance spectra of polycrystalline $O_2^+BF_4^-$, $O_2^+AsF_6^-$, $O_2^+SbF_6^-$, and $O_2^+Sb_2F_{11}^-$ were recorded over the temperature range −190 to +20° at 9.35 GHz. The *g* tensors calculated from simulated spectra of $O_2^+BF_4^-$, $O_2^+AsF_6^-$, and $O_2^+Sb_2F_{11}^-$ at −196° indicated the ions are in sites of orthorhombic or lower symmetry. Two of the components of the *g* tensor were between 1.96 and 2.00. The third component was between 1.73 and 1.76 in agreement with crystal field theory. The line shapes were lorentzian indicating that dipolar broadening is at least partially averaged by thermal motion. Above −196°, the line widths of the spectra increased rapidly indicating a relaxation process which has a small activation barrier. The spectrum of $O_2^+SbF_6^-$ was very broad at −196° and exhibited additional lines of magnetic fields in the region of 1000–1500 G. This may be due to strong exchange between nearest $O_2^+$ ions. An improved synthesis of $O_2^+BF_4^-$ was described involving low-temperature uv photolysis of a $BF_3$–$F_2$–$O_2$ mixture.

## Introduction

The preparation of a variety of dioxygenyl salts has been reported.[1,2] Although electron spin resonance (esr) has been used to confirm the paramagnetic character of dioxygenyl tetrafluoroborate[3,4] and hexafluoroarsenate,[5] no interpretations of these spectra have been reported. An esr spectrum was reported for $O_2^+BF_4^-$ at −196° consisting of one asymmetric line with a peak to peak line width ($\Delta H_{pp}$) between 400 and 500 G and a *g* factor between 1.94 and 1.97.[3,4] The spectrum reported for $O_2^+AsF_6^-$ was characterized by a *g* factor of 1.9880 ± 0.0002 and a temperature-dependent line width of 24 G at −50° and 66 G at 23°.[5] Both the $BF_4^-$ and the $AsF_6^-$ anions are large such that both materials would be expected to exhibit similar spectra. Recently, esr spectra of $O_2^+SbF_6^-$, $O_2^+AsF_6^-$, and $O_2^+Sb_2F_{11}^-$ at temperatures near liquid helium were studied. These spectra were interpreted in terms of near-axial symmetry.[6] Values of $g_\perp$ were about 1.97 and those of $g_\parallel$ were 1.73. In addition, the magnetic susceptibility of these salts and the $^{19}F$ nmr of $O_2^+AsF_6^-$ were reported.[6]

Esr spectra of concentrated paramagnetic samples generally exhibit a variety of relaxation processes. Dipolar broadening results from the various magnetic fields generated by the close magnetic dipoles acting on the central ion. Exchange processes, cross relaxation, or motion of the magnetic ion can also cause a modulation of the magnetic energy levels and therefore relax the spin states. The $O_2^+$ ion has the additional possibility of Jahn–Teller relaxation since it is in a nearly degenerate state. In a crystal field which is symmetric with respect to the internuclear axis, two states are separated only by the spin–orbit coupling energy (about 200 $cm^{-1}$). These effects have not been considered in the interpretation of the esr spectra of compounds of $O_2^+$.

Esr spectra have been observed for $O_2^+$ and the isoelectronic species $N_2^-$ and NO in single crystals and adsorbed on surfaces. Detailed studies of $O_2^+$ on rutile surfaces,[7] $N_2^-$ in single crystals of irradiated azides,[8] and nitric oxide adsorbed on various surfaces[9–11] and generated by irradiation in azides[12] have been reported. Nitric oxide in single crystals and on some surfaces exhibits spectra characteristic of a three-component *g* tensor when the line widths are sufficiently narrow so that all components can be resolved. On some surfaces NO exhibits a spectrum with a broad-line characteristic of apparent axial symmetry; however, simulations assuming axial symmetry do not accurately reproduce the spectra.

Synthetic aspects add further interest to this study. Recent communications[13,14] indicate that the previously reported photochemical synthesis of $O_2^+SbF_6^-$ results in a product which contains appreciable amounts of the dimeric anion $Sb_2F_{11}^-$. In addition, no convenient synthesis has been reported for the preparation of $O_2^+BF_4^-$.

In view of the discrepancies in the esr spectra of $O_2^+$ and for the purpose of understanding the behavior of $O_2^+$ in a crystalline environment, we have investigated the esr spectra of this ion in the presence of several counterions. In addition, an improved synthesis is reported for $O_2BF_4$.

## Experimental Section

**Preparation of $O_2^+$ Salts.** The $O_2^+AsF_6^-$ and $O_2^+SbF_6^-$ samples were prepared at 200° from $O_2$, $F_2$, and $AsF_5$ or $SbF_5$, respectively, in Monel cylinders according to the method of Beal, *et al.*[15] Material balances, vibrational spectra,[16] and elemental analyses (oxygen content was determined by displacemeent reaction with excess FNO at −78° and As or Sb were determined by conventional techniques) showed that the solid products had the compositions $O_2^+AsF_6^-$ and $O_2^+SbF_6^-\cdot 0.06SbF_5$, respectively. A sample having the composition $O_2^+SbF_6^-\cdot 0.73SbF_5$ was prepared by the above method but by heating the starting materials to 150° for 12 hr. A sample of $O_2^+Sb_2F_{11}^-$ was prepared by uv photolysis of a 1:1/2:2 mole ratio mixture of $O_2$–$F_2$–$SbF_5$ in a manner similar to that described by McKee and Bartlett.[14]

For the synthesis of $O_2^+BF_4^-$, a 1-l. Pyrex bulb containing equimolar amounts of $O_2$, $F_2$, and $BF_3$, at a total pressure of 800 mm, was exposed for 7 days to uv radiation from a high-pressure mercury lamp (Hanovia 616A, 100 W) equipped with a water filter. The condensing tip of the reactor was kept at −78°. The solid $O_2^+BF_4^-$ accumulated in the cold section of the reactor and was periodically removed at 0° from the walls to the bottom of the reactor by means of an ultrasonic cleaning bath. After completion of the photolysis, products volatile at −78° were removed *in vacuo*. The white solid residue was transferred, while cold, from the Pyrex container to a Teflon–FEP ampoule in an inert-atmosphere glove box. Vibrational spectroscopy[17] and elemental analysis (see above) showed the product to be $O_2^+BF_4^-$. The yield was 51%.

**Esr Spectra.** Esr spectra were obtained on a modified Varian V-4502 dual-cavity esr spectrometer.[18] The magnetic field was monitored using a sample of $Mn^{2+}$ in forsterite.[19] Each of the six lines from the $Mn^{2+}$ were narrower than 1.5 G, and the splittings and the *g* factor were determined against DPPH ($g = 2.00365$) using a proton resonance probe to calibrate the magnetic field. The esr parameters for $Mn^{2+}$ were $g = 2.00095 \pm 0.00006$ and $a = 86.75 \pm 0.05$ G. To calibrate the field difference from the field corresponding to $g_{Mn^{2+}}$ for each manganous line, the hyperfine Hamiltonian was expanded to second order.

The reference channel was operated at 100-kHz field modulation, and the sample channel was operated at 14.7-kHz with a set of water-cooled coils which allow peak-to-peak modulation amplitudes up to 100 G.[20] In all spectra, the modulation amplitude was less 0.1 of the peak-to-peak line width of the spectrum. Simulations of the powder spectra were carried out by the method of Griscom, Taylor, Ware, and Bray[21] on a CDC 6600 computer with a Calcomp plotter. Three components of a *g* tensor were required to simulate the spectra. Since two components were very close ($g_x$ and $g_y$) and one componeent

* To whom correspondence should be addressed at the Science Center.

**Table I.** Esr Parameters of Dioxygenyl Compounds at −196°

| | $g_x$ | $g_y$ | $g_z$ | $\Delta H_{pp}$,[a] G | $\Delta$,[b] $cm^{-1}$ | $10^4E$,[b] $cm^{-1}$ |
|---|---|---|---|---|---|---|
| $O_2AsF_6$ | 2.000 | 1.973 | 1.742 | 80 | 1480 | 1.00 |
| $O_2BF_4$ | 2.00 | 1.98 | 1.78 | 260 | 1500 | 2.0 |
| $O_2SbF_6$ | 1.75 | Isotropic | | 2200 | | |
| $O_2Sb_2F_{11}$ | 1.970 | 1.958 | 1.729 | 120 | 1960 | 1.20 |

[a] Lorentzian line width used to simulate the powder spectrum. [b] Parameters derived from $g$ factors assuming $\lambda = 195$ $cm^{-1}$.

($g_z$) was at considerably higher fields, the dependence of magnetic field on the intensity was treated by the relationship

$$I \propto \left(\frac{g_x + g_y}{2}\right)^2\left[\left(\frac{gz}{g}\right)^2 + 1\right]$$

where $I$ is the intensity and $g$ is the apparent $g$ factor given by $h\nu/\beta H$. This is analogous to the relationship derived by Bleaney.[22]

Samples of the dioxygenyl salt were placed in 4-mm Teflon–FEP or quartz tubes and heat sealed. The Teflon–FEP tubes exhibited a weak spectrum of two lines each about 1 G wide, at points very close to $g = 2$. Under the high powers and high modulation amplitudes used, these lines were broadened and weakened even further. At liquid nitrogen temperatures where large signals were observed, low gains and small modulation amplitudes were used and the Teflon–FEP spectrum was too weak to be detected. Samples prepared in Monel vessels exhibited a weak line about 20 G wide at −196°. This is probably due to a copper or nickel ion impurity. This signal is similar to that previously reported for $O_2^+AsF_6^-$.[5] The samples of antimonates and the arsenates were stored for several weeks at room temperature with no noticeable decrease of signal intensity. The tetrafluoroborate salts were stored at −20° and were also stable for several weeks.

## Results and Discussion

**Syntheses of $O_2^+$ Salts.** The previous reports on the photochemical synthesis[5] of $O_2^+AsF_6^-$ and the thermal synthesis[15] of $O_2^+SbF_6^-$ were confirmed. For the thermal synthesis of $O_2^+SbF_6^-$ it was found important to keep the reaction temperature sufficiently high, *i.e.*, at about 200°, in order to suppress the formation of $O_2^+Sb_2F_{11}^-$. A reasonable explanation for this temperature requirement is the melting point of $O_2^+Sb_2F_{11}^-$ which was recently reported[12] to be 180–185°. Below 180°, $O_2^+Sb_2F_{11}^-$ can solidify thus escaping further interaction with $O_2$ and $F_2$.

The uv photolysis of $O_2$–$F_2$–$SbF_5$ mixtures yields mainly $O_2^+Sb_2F_{11}^-$ and not $O_2^+SbF_6^-$ as originally reported.[5] This finding is in excellent agreement with a recent study by McKee and Bartlett.[14] Since the esr spectra of $O_2^+SbF_6^-$ and $O_2^+Sb_2F_{11}^-$ (see below) strongly differ, they are useful for distinguishing the two compounds.

The previously reported syntheses[1] of $O_2^+BF_4^-$ required oxygen fluorides, such as $O_2F_2$ or $O_4F_2$, as starting materials. Since these oxygen fluorides are difficult to prepare (low-temperature glow discharge, $\gamma$ irradiation, or photolysis) and, owing to their thermal instability, inconvenient to handle, a direct synthesis from $O_2$, $F_2$, and $BF_3$ appeared desirable. We have found that $O_2^+BF_4^-$ can easily be prepared by uv photolysis of $O_2$–$F_2$–$BF_3$ mixtures. During this photolysis part of the reactor must be kept at −78° to avoid thermal decomposition of the product which is of only marginal thermal stability at ambient temperature. Our yield (~50%) of $O_2^+BF_4^-$ and conversion rates could probably be significantly improved by choosing a reactor geometry more favorable than the cold-finger Pyrex bulb used in our experiment.

**Observed Spectra.** Parameters determined from the esr spectra of $O_2^+$ compounds are given in Table I. Although the spectra of $O_2^+Sb_2F_{11}^-$ and $O_2^+AsF_6^-$ at −196° appear characteristic of radicals with axial symmetry, the spectra cannot be accurately simulated unless three independent $g$ factors are used. The experimental and computed spectra of $O_2^+AsF_6^-$ are shown in Figure 1. The spectrum of $O_2^+BF_4^-$

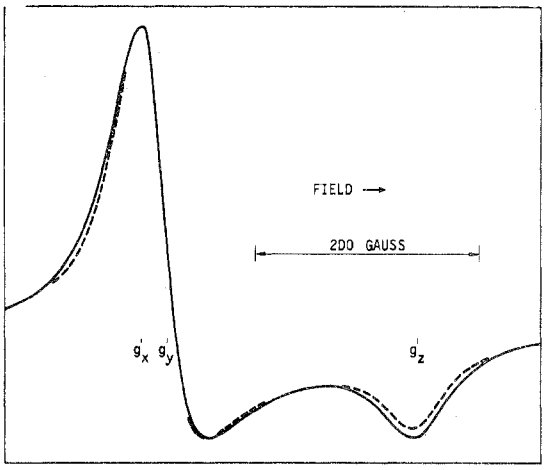


**Figure 1.** Esr spectrum of dioxygenyl hexafluoroarsenate at −196° (solid line) and computer simulation using the parameters $g_x = 2.000$, $g_y = 1.973$, $g_z = 1.742$, and $\Delta H_{pp} = 80$ G (broken line).

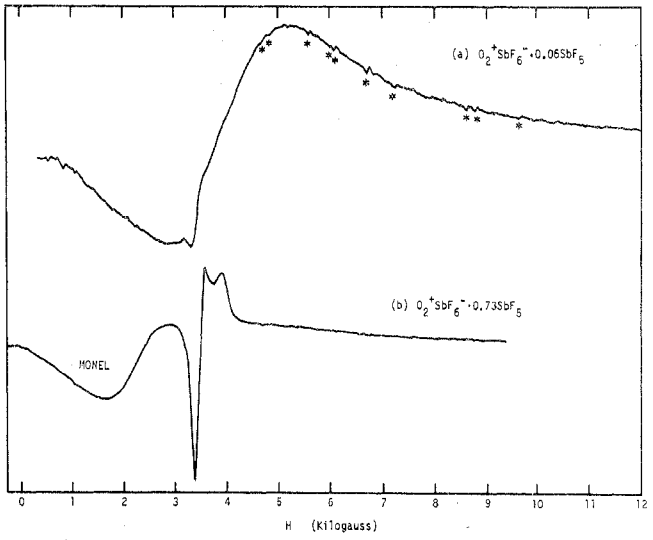


**Figure 2.** Esr spectra of dioxygenyl fluoroantimonates at −196° (frequency 9.317GHz): (a) sample of composition $O_2^+SbF_6^-\cdot 0.06SbF_5$; (b) sample of composition $O_2^+SbF_6^-\cdot 0.73SbF_5$.

is similar to that described in the literature.[3,4] We observe an asymmetric line with a peak-to-peak width of 430 G. Parameters shown in Table I were determined assuming orthorhombic symmetry. Due to the low resolution of this spectrum, those parameters are not particularly accurate. The spectrum of $O_2^+SbF_6^-$ at −196° appears isotropic with a $g$ factor of about 1.75 and a line width of 2200 G. This spectrum and the spectrum of $O_2^+SbF_6^-\cdot 0.73SbF_5$ are shown in Figure 2. Lines due to gaseous molecular oxygen are identified by an asterisk. The spectrum of $O_2^+SbF_6^-\cdot 0.73SbF_5$ exhibits two components: one component is very broad, and the second component is similar to the spectra of $O_2^+Sb_2F_{11}^-$ and $O_2^+AsF_6^-$. The broad component in the spectrum of $O_2^+SbF_6^-\cdot 0.73SbF_5$ is considerably different from the spectrum of $O_2^+SbF_6^-$. These samples were prepared in Monel which exhibits magnetic behavior. Esr spectra of scrapings from different parts of the bomb were recorded and the spectra showed considerable variation. The line widths varied between 700 and 1100 G and the field corresponding to the mean amplitude between maximum and minimum peaks of the derivative varied between 2100 and 2500 G. It is therefore likely that the low-field component in Figure 2b is due to Monel. Apparently the Monel contributes little to the spectrum shown in Figure 2a.

The line widths of the spectra of $O_2^+BF_4^-$, $O_2^+AsF_6^-$, and

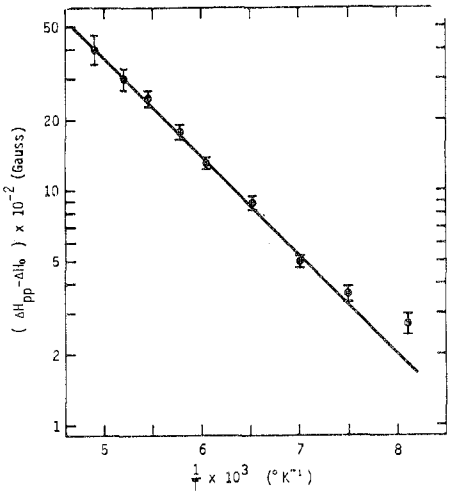


**Figure 3.** Temperature dependence of the line width of the esr spectrum of dioxygenyl hexafluoroarsenate.

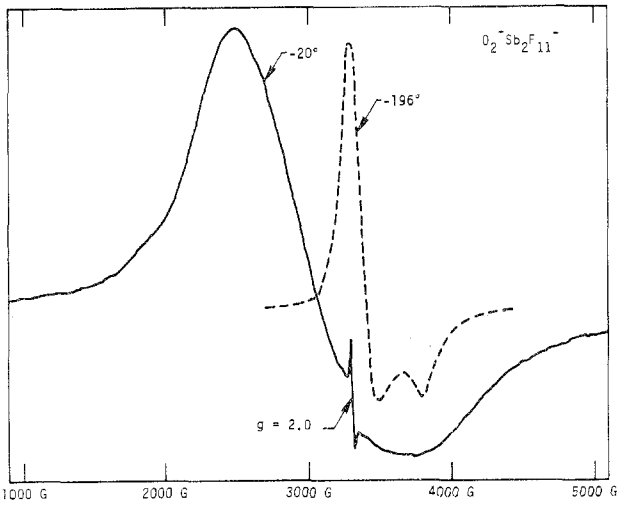


**Figure 4.** Comparison of esr spectra recorded at −196° (broken line) and −20° (solid line) of $O_2^+Sb_2F_{11}^-$ prepared in quartz. Signal at $g = 2$ is due to an undetermined impurity.

$O_2^+Sb_2F_{11}^-$ and the narrow component of the spectrum of $O_2^+SbF_6^-\cdot 0.73SbF_5$ increase rapidly at temperatures greater than −170°. The line width of $O_2^+AsF_6^-$ exhibits an exponential dependence on $1/T$ between −160 and −70° as shown in Figure 3. The spectrum of $O_2^+BF_4^-$ appears to behave in a similar way; however within a few degrees of −130° the spectrum disappears when warmed and reappears when cooled. This suggests that a crystal modification occurs at this temperature.

The compounds $O_2^+Sb_2F_{11}^-$, $O_2^+SbF_6^-$, and $O_2SbF_6^-\cdot 0.73SbF_5$ exhibit different temperature dependences. At −165° the spectrum of $O_2^+Sb_2F_{11}^-$ is broadened and a low-field shoulder begins to appear. As the temperature is increased, the original component broadens out, and an asymmetric line with an apparent $g$ factor of 2.3 emerges from the shoulder. Above −100°, only the "$g = 2.3$" line can be detected as shown in Figure 4. This sample was not prepared in Monel.

The spectrum of $O_2^+SbF_6^-$ at −196° is very broad with $\Delta H_{pp}$ about 2300 G and a $g$ factor of 1.75. At higher fields, this absorption shifts to higher fields and low-field shoulders emerge. These absorptions become defined at −60° with apparent $g$ factors of 4.69 and 2.83 for the low-field absorptions and approximately 0.9 for the high-field absorption. The high-field absorption can be ascribed to the $O_2^+$ in which the angular momentum is virtually unquenched. The absorption at $g = 2.83$ is probably due to Monel. The absorption of $g = 4.69$ broadens with temperature. The spectrum of $O_2^+SbF_6^-\cdot 0.73SbF_5$ (Figure 2b) exhibits two components. At temperatures above −196° the sharper component is again broadened. At 20°, only an 800 G wide absorption at $g = 2.80$ can be seen which is probably due to Monel. All spectra described here are reversible as the temperature is increased or decreased.

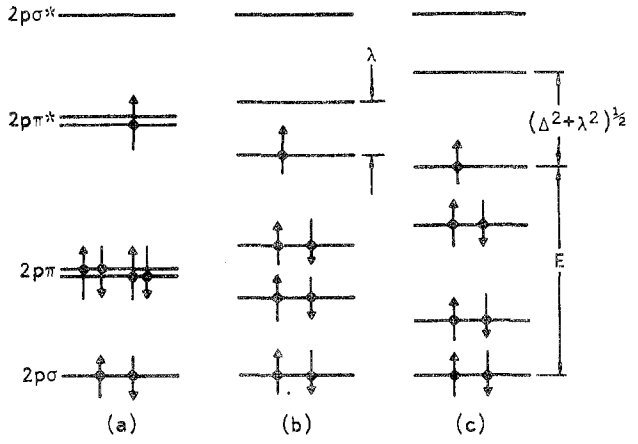


**Figure 5.** Energy level diagram of the dioxygenyl ion showing the $\sigma$- and $\pi$-bonding 2p orbitals: (a) energy levels in the absence of spin–orbit coupling and crystal field effects; (b) energy levels with spin–orbit splitting; (c) energy levels with spin–orbit and orthorhombic field splittings.

**g Tensor.** In the absence of spin–orbit coupling and crystal field effects, the dioxygenyl ion would be in a degenerate state, and the energy level diagram would be given by Figure 5a. Spin–orbit coupling splits the energy levels of the $2p\pi$ and $2p\pi^*$ states (Figure 5b). The application of an orthorhombic crystal field further separates the energy levels and quenches the angular momentum (Figure 5c)). Crystal field calculations were carried out in a manner similar to that described by Mergerian and Marshall.[12] The matrix elements of the crystal field potential operator $V_{cf}$ are given by eq 1 where Dirac

$$\langle M_l', M_s' | V_{cf} | M_s M_l \rangle = \Delta \delta_{M_s M_s'} \delta_{M_l \pm 1, M_l'} \quad (1)$$

notation is used, $M_l$ and $M_s$ are the azimuthal quantum numbers for the angular momentum and spin, $\delta$ is the Dirac $\delta$ function, and $\Delta$ is the magnitude of the crystal field energy. The $\pi$ and $\pi^*$ levels consist of values of $M_l$ which are equal to +1 or −1. The spin–orbit coupling operator only has diagonal elements equal to $\lambda M_l M_s$.

The solution of the secular determinant gives the energies of either the $2p\pi$ or $2p\pi^*$ states relative to the energy of the unsplit levels. Each of the two states which result are degenerate in spin, and the energies are given in eq 2.

$$E_1 = {}^1/_2(\Delta^2 + \lambda^2)^{1/2} \quad (2a)$$

$$E_2 = -{}^1/_2(\Delta^2 + \lambda^2)^{1/2} \quad (2b)$$

The wave functions which correspond to these energies are

$$\Psi_{1\alpha}^{\circ} = N_1\left(|1, {}^1/_2\rangle - \left\{\frac{\lambda}{\Delta} - \left[1 + \left(\frac{\lambda}{\Delta}\right)^2\right]^{1/2}\right\}|-1, {}^1/_2\rangle\right) \quad (3a)$$

$$\Psi_{1\beta}^{\circ} = N_2\left(|1, -{}^1/_2\rangle + \left\{\frac{\lambda}{\Delta} + \left[1 + \left(\frac{\lambda}{\Delta}\right)^2\right]^{1/2}\right\}|-1, -{}^1/_2\rangle\right) \quad (3b)$$

$$\Psi_{2\alpha}^{\circ} = N_2\left(|1, {}^1/_2\rangle - \left\{\frac{\lambda}{\Delta} + \left[1 + \left(\frac{\lambda}{\Delta}\right)^2\right]^{1/2}\right\}|-1, {}^1/_2\rangle\right) \quad (3c)$$

$$\Psi_{2\beta}^{\circ} = N_1\left(|1, -{}^1/_2\rangle - \left\{\frac{\lambda}{\Delta} - \left[1 + \left(\frac{\lambda}{\Delta}\right)^2\right]^{1/2}\right\}|-1, -{}^1/_2\rangle\right) \quad (3d)$$

where $N_1$ and $N_2$ are normalization constants given by

$$N_1 = \left(2\left[1+\left(\frac{\lambda}{\Delta}\right)^2\right]^{1/2}\left\{\left[1+\left(\frac{\lambda}{\Delta}\right)^2\right]^{1/2}-\frac{\lambda}{\Delta}\right\}\right)^{-1/2} \quad (4a)$$

$$N_2 = \left(2\left[1+\left(\frac{\lambda}{\Delta}\right)^2\right]^{1/2}\left\{\left[1+\left(\frac{\lambda}{\Delta}\right)^2\right]^{1/2}+\frac{\lambda}{\Delta}\right\}\right)^{-1/2} \quad (4b)$$

The $O_2^-$ ion behaves in a similar way and exhibits the same crystal field splittings. The difference between $O_2^-$ and $O_2^+$ is that the unpaired electron of $O_2^-$ is considered to be in the state corresponding to energy $E_1$, while the unpaired electron of $O_2^+$ is considered to be in the state corresponding to energy $E_2$.

The $g$ tensor for the dioxygenyl ion may be calculated by the method of Kanzig, *et al.*[23] An additional term which contributes to the $2p\pi^*$ levels arises from interaction with the $2p\sigma$ levels. This results in a small admixture of $-1/2$ spin to wave functions which are predominantly of $+1/2$ spin, and a small admixture of $+1/2$ spin to the wave functions which are predominantly $-1/2$ spin. The additional term added to eq 3c is of the form $(\lambda/E)|0, -1/2\rangle$, and the term added to eq 3d is of the form $(\lambda/E)|0, 1/2\rangle$. Using second-order perturbation theory, the additional terms added to the basis wave functions are shown in eq 5.

$$\Psi_{2\alpha}' = \Psi_{2\alpha}^\circ - \frac{\lambda}{2E}\frac{\left\{\frac{\lambda}{\Delta}+\left[1+\left(\frac{\lambda}{\Delta}\right)^2\right]^{1/2}\right\}^{1/2}}{\left[1+\left(\frac{\lambda}{\Delta}\right)^2\right]^{1/2}}|0, -1/2\rangle \quad (5a)$$

$$\Psi_{2\beta}' = \Psi_{2\beta}^\circ + \frac{\lambda}{2E}\frac{1}{\left[1+\left(\frac{\lambda}{\Delta}\right)^2\right]^{1/2}\left\{\left[1+\left(\frac{\lambda}{\Delta}\right)^2\right]^{1/2}-\frac{\lambda}{\Delta}\right\}}|0, 1/2\rangle \quad (5b)$$

The $g$ factors can now be calculated using the magnetic Hamiltonian. Fields are independently assumed along the $x$, $y$, or $z$ axes of the dioxygenyl ion.

In the absence of the $M_l = 0$ functions, only the wave functions are coupled through $\hat{S}_+$ and $\hat{S}_-$. The addition of the $M_l = 0$ functions allows coupling through $\hat{L}_+$ and $\hat{L}_-$. The $g$ factors are obtained by diagonalizing the $2 \times 2$ matrices formed by application of $H_{mag}$. This procedure is outlined in more detail by Wertz and Bolton.[24]

The results of these calculations are given in eq 6 which

$$g_z = g_e - 2\left(\frac{\lambda^2}{\lambda^2+\Delta^2}\right)^{1/2} \quad (6a)$$

$$g_x = g_e\left(\frac{\Delta^2}{\lambda^2+\Delta^2}\right)^{1/2} - \frac{\lambda}{E}\left[\left(\frac{\Delta^2}{\lambda^2+\Delta^2}\right)^{1/2}+\left(\frac{\lambda^2}{\lambda^2+\Delta^2}\right)^{1/2}+1\right] \quad (6b)$$

$$g_y = g_e\left(\frac{\lambda^2}{\lambda^2+\Delta^2}\right)^{1/2} + \frac{\lambda}{E}\left[\left(\frac{\lambda^2}{\lambda^2+\Delta^2}\right)^{1/2}-\left(\frac{\lambda^2}{\lambda^2+\Delta^2}\right)^{1/2}-1\right] \quad (6c)$$

shows that the **g** tensor should be comprised of three different principal values provided that $E$ is sufficiently small.

**Crystal Field Effects.** The esr parameters determined from the simulations, which are given in Table I, can be used to calculate the parameters $\Delta$ and $E$ shown in Figure 5. The $g$ factors of $O_2^+AsF_6^-$ and $O_2^+Sb_2F_{11}^-$ are believed accurate to $\pm 0.002$, and that of $O_2^+BF_4^-$ is believed accurate to $\pm 0.02$. There is some doubt of the spin–orbit coupling constant $\lambda$ of $O_2^+$ in a crystal lattice. The values of $\lambda$ are 195 $cm^{-1}$ for the free ion[25] and 151 $cm^{-1}$ for atomic oxygen. Since the crystal field probably reduces the value of $\lambda$ from the free ion, the correct value is probably between 151 and 195 $cm^{-1}$. In principle, the value of $\lambda$ can also be determined from the solutions of the simultaneous equations (6a)–(6c), but the precision of the $g$ factors is not sufficiently accurate for this purpose. Arbitrarily, the free-ion value of $\lambda$ was used. The values of $\Delta$ and $E$ which are given in Table I must therefore be considered as upper limits of these energies.

These values can be compared with those determined from spectra of $O_2^-$ and the isoelectronic NO. The comparison of the crystal field parameters of $O_2^+$ and $O_2^-$ is valid since a similar mixing of orbitals takes place to give shifts of the $g$ factor from $g_e$. In NaI where large negative ions and small positive ions surround the $O_2^-$ ion, the angular momentum is unquenched.[23] However, in other halides[23] values of $\Delta$ range from 650 to 1200 $cm^{-1}$ and values of $E$ range from $6 \times 10^4$ to $15 \times 10^4$ $cm^{-1}$. The precise values depended upon the sizes of the ions and the symmetry of the lattice sites. The asymmetry was attributed to covalent interaction between the $O_2^-$ and the alkali metal ions since the site of the $O_2^-$ ion aligns in the 110 direction such that the crystal ions are axially symmetric with respect to the $O_2^-$ internuclear axes. In other studies, alkali metal–$O_2^-$ compounds were trapped in an argon matrix at 4°K,[26,27] so that the principal interaction is with one alkali metal ion. In these cases $\Delta$ for $O_2^-$ was considerably larger than in alkali metal halides.

Values of $\Delta$ and $E$ obtained for NO adsorbed on various zeolites agree more closely with the values obtained here for $O_2^+$. Values of $\Delta$ range from 1050 to 1700 $cm^{-1}$, and values of $E$ range between $1.2 \times 10^4$ and $3.7 \times 10^4$ and are consistent with a small interaction with the surface.[9] NO adsorbed on MgO and generated in various crystals exhibits larger values of $\Delta$ and $E$, and thus the elements of the **g** tensor are much closer to $g_e$.[10] Similarly, the $N_2^-$ generated in $KN_3$[8] is also in sites with greater asymmetry and exhibits $g$ factors closer to $g_e$.

The data of Table I suggest that in $O_2^+BF_4^-$, $O_2^+AsF_6^-$, and $O_2^+Sb_2F_{11}^-$, the $O_2^+$ cation is in the site of a small orthorhombic field. The origin of the field can be due either to covalent interaction with the fluorine in the complex anion, as suggested from neutron diffraction studies on $O_2^+PtF_6^-$[28] or to an asymmetric arrangement of anions around $O_2^+$. Values of $\Delta$ were also estimated from magnetic susceptibility measurements.[6] If a value for $\lambda$ of 195 $cm^{-1}$ is assumed, then $\Delta$ would be about 1400 $cm^{-1}$.

Measurements of the spectrum of $O_2^+SbF_6^-$ at −250°[6] indicate that the spectrum is sharpened considerably when the temperature is below −195°, and the $O_2^+$ ion may also be in an orthorhombic environment.

**Temperature Dependence.** The spectra of each of the $O_2^+$ compounds exhibit a strong temperature dependence. In all samples studied, as the temperature is increased, the lines broaden. Only $O_2^+AsF_6^-$ exhibited a spectrum with a single component over a sufficiently large temperature range so that the line width can be investigated as a function of temperature. $O_2^+BF_4^-$ was assumed to be linear over a narrow range of temperature. If the slopes of $\ln(\Delta H_{pp} - \Delta H_0)$ *vs.* $1/T$ for $O_2^+AsF_6^-$ and $O_2^+BF_4^-$ are considered to be related to activation energies in an Arrhenius plot, the energy for the relaxation of the spectrum of $O_2^+AsF_6^-$ is 1.92 kcal (690 $cm^{-1}$) and that of $O_2^+BF_4^-$ is 1.3 kcal (470 $cm^{-1}$). These values are considerably smaller than the crystal field energies calculated from the $g$ factors and suggest that there may be several modes operating to cause relaxation.

Since cross relaxation and exchange interactions are possible modes of relaxations in concentrated paramagnetic samples, attempts were made to form dilute $O_2^+$ salts in an $NO^+AsF_6^-$ lattice. The simultaneous formation of $NO^+AsF_6^-$ was

unsuccessful since the reaction of NO + $F_2$ + $AsF_5$ is much faster than that of $O_2$ + $F_2$ + $AsF_5$. The displacement of $O_2^+$ by $NO^+$ by exposing $O_2^+AsF_6^-$ to FNO at −77° did not produce the desired cation distribution.

The mechanism of the relaxation process cannot be determined from line width measurements alone since the components of spin–lattice and spin–spin relaxation times cannot be separated. At line widths in the order of 100 G an incident microwave power far in excess of the Klystron output would be required in order to use progressive saturation techniques. Based on other measurements we can speculate on the relaxation mechanism.

Calculations of the dipolar broadening based on the published crystal structure of the dioxygenyl compounds[14,29,30] were carried out according to the model of Van Vleck.[31] In all cases the second moment was about $10^4$ $G^2$. If this is the dominant broadening mechanism, the powder spectrum should be simulated by convoluting the powder spectrum onto a gaussian line shape with a width of more than 100 G peak-to-peak. However, for $O_2AsF_6^-$ and $O_2^+Sb_2F_{11}^-$ lorentzian lines were required. This result indicates that at least some of the dipolar interactions are partially averaged in the lattice even at −196°.

Recent $^{19}F$ nmr studies of $O_2^+AsF_6^-$ indicate substantial cation motion in the lattice at temperatures above −240°.[6] A similar conclusion was derived from electron diffraction studies of $O_2^+PtF_6^-$.[28] These results suggest that modulation of the crystal field energy[32] is indeed one reasonable mechanism for relaxation of the electron spin. Although the spectrum of $O_2^+SbF_6^-$ is extremely broad at −196°, cooling further sharpens the line.[6] This further suggests that in this lattice there is more room for motion of the $O_2^+$ ion. $O_2^+BF_4^-$ is also somewhat broader than $O_2^+AsF_6^-$ and $O_2^+Sb_2F_{11}^-$ although the crystal field is stronger. In the $O_2^+BF_4^-$ lattice, the $O_2^+$ ions are closer, and it is more likely that exchange processes are more significant than in the other materials as a means of relaxation. This would also explain the apparently smaller activation energy.

In the three dioxygenyl–antimonate compounds studied, different low-field absorptions appear at temperatures greater than −130°. This may be the result of strong exchange interactions between neighboring $O_2^+$ ions. This exchange process may also account for part of the more rapid relaxation of $O_2^+$ at −196°. One mechanism which may account for the enhanced exchange in the antimonates would be one wherein the $SbF_6^-$ ion acts as a bridge between $O_2^+$ ions. This is more likely in antimonates than in any of the other materials studied since the antimonates are more polarizable. Figure 4 shows the spectrum of $O_2^+Sb_2F_{11}^-$ at −20°. An asymmetric line with an apparent $g$ factor of 2.3 can be seen.

Although these processes are not completely understood, the different spectra of $O_2^+Sb_2F_{11}^-$ and $O_2^+SbF_6^-$ at −196° appear to be a simple, nondestructive qualitative method to detect the presence of $Sb_2F_{11}^-$ formed in $O_2^+SbF_6^-$ during synthesis. Figure 2a demonstrates that amounts of $Sb_2F_{11}^-$ as low as about 5% can be readily detected by esr.

## Conclusions

1. $g$ factors of $O_2^+AsF_6^-$, $O_2^+Sb_2F_{11}^-$, and $O_2^+BF_4^-$ indicate strong orthorhombic symmetry around the $O_2^+$ ion in the lattice.

2. Values for the orthorhombic crystal field and for the energy separation between $\sigma$ and $\pi^*$ states are in agreement with values of $O_2^-$ and NO in single crystals and NO adsorbed on zeolites.

3. Several different relaxation processes to account for the temperature dependence of the line width of the esr spectra were proposed. Modulation of the crystal field by ion motion appears to be a dominant mechanism. The spectrum of $O_2^+SbF_6^-$ undergoes faster relaxation at −196° than each of the other salts.

4. Anomalous spectra for dioxygenyl antimonates above −140° were observed. Absorptions where $g > 2$ may indicate coupling between dioxygenyl ions.

5. Because of the difference between spectra of $O_2^+SbF_6^-$ and $O_2^+Sb_2F_{11}^-$ or $O_2^+SbF_6^-$·0.73$SbF_5$ at −196°, esr can be used to demonstrate the absence of excess $SbF_5$ in $O_2^+SbF_6^-$.

**Acknowledgment.** The portion of this work carried out at the Rocketdyne Division of Rockwell International was supported by the Office of Naval Research, Power Branch. We are indebted to Drs. D. Pilipovich, L. Grant, and C. J. Schack for helpful discussions and to Dr. W. E. Falconer for communicating his results to us prior to publication.

**Registry No.** $O_2AsF_6$, 12370-43-3; $O_2BF_4$, 12228-13-6; $O_2SbF_6$, 12361-66-9; $O_2Sb_2F_{11}$, 12592-38-0.

## References and Notes

(1) I. V. Nikihin and V. Ya. Rosolovskii, *Russ. Chem. Rev.*, **40**, 889 (1971); *Usp. Khim.*, **40**, 1913 (1971), and ref cited therein.
(2) A. J. Edwards, W. E. Falconer, J. E. Griffiths, W. A. Sunder, and M. J. Vasile, *J. Chem. Soc., Dalton Trans.*, 1129 (1974).
(3) C. T. Goetschel, V. A. Campanile, C. D. Wagner, and J. N. Wilson, *J. Amer. Chem. Soc.*, **91**, 4702 (1969).
(4) I. J. Solomon, R. J. Brabets, R. K. Uenishi, J. N. Keith, and J. M. McDonough, *Inorg. Chem.*, 3, 457 (1964).
(5) J. Shamir and J. Binenboym, *Inorg. Chim. Acta*, **2**, 37 (1968).
(6) F. J. DiSalvo, W. E. Falconer, R. S. Hutton, A. Rodriguez, and J. V. Waszcak, submitted for publication in *J. Chem. Phys.*
(7) R. D. Iyengar, M. Codell, J. S. Karra, and J. Turkevich, *J. Amer. Chem. Soc.*, **88**, 5055 (1966); R. D. Iyengar and R. Kellerman, *J. Colloid Interface Sci.*, **35**, 424 (1971).
(8) E. Gelerinter and R. H. Silsbee, *J. Chem. Phys.*, **45**, 1703 (1966); E. Gelerinter, *ibid.*, **53**, 2991 (1970); B. Ford and E. Gelerinter, *ibid.*, **55**, 3660 (1971).
(9) C. L. Gardiner and M. A. Weinberger, *Can. J. Chem.*, **48**, 1317 (1970).
(10) J. H. Lunsford, *J. Chem. Phys.*, **46**, 4347 (1967); *J. Phys. Chem.*, **72**, 4163 (1968); **74**, 1518 (1970); *J. Catal.*, **14**, 379 (1969); M. Primet, *J. Chim. Phys. Physicochim. Biol.*, **67**, 1629 (1970); C. Naccache, M. Che, and Y. Ben Taarit, *Chem. Phys. Lett.*, **13**, 109 (1972); B. M. Hoffman and N. J. Nelson, *J. Chem. Phys.*, **50**, 2598 (1969).
(11) M. Che, J. Vedrine, and C. Naccache, *Bull. Soc. Chim. Fr., Suppl.*, 121 (1970).
(12) D. Mergerian and S. A. Marshall, *Phys. Rev.*, **127**, 2015 (1962).
(13) Z. K. Nikitina and V. Ya. Rosolovskii, *Bull Acad. Sci. USSR, Div. Chem. Sci.*, **10**, 2048 (1970).
(14) D. E. McKee and N. Bartlett, *Inorg. Chem.*, **12**, 2738 (1973).
(15) J. B. Beal, Jr., C. Pupp, and W. E. White, *Inorg. Chem.*, **8**, 828 (1969).
(16) J. Shamir, J. Binenboym, and H. H. Claassen, *J. Amer. Chem. Soc.*, **90**, 6223 (1968).
(17) K. R. Loos, V. A. Campanile, and C. T. Goetschel, *Spectrochim. Acta, Part A*, **26**, 365 (1970).
(18) I. B. Goldberg and W. F. Goeppinger, *Inorg. Chem.*, **11**, 3129 (1972).
(19) G. K. Miner, T. P. Graham, and G. T. Johnston, *Rev. Sci. Instrum.*, **43**, 1297 (1972).
(20) I. B. Goldberg, A. J. Lewin, and J. R. Crandall, *Rev. Sci. Instrum.*, **45**, 855 (1972).
(21) D. L. Griscom, P. C. Taylor, D. A. Ware, and P. J. Bray, *J. Chem. Phys.*, **48**, 5158 (1968); P. C. Taylor and P. J. Bray, *J. Magn. Resonance*, **2**, 305 (1970).
(22) B. Bleaney, *Proc. Phys. Soc., London, Sect A*, **63**, 407 (1958); *Proc. Phys. Soc., London*, **75**, 621 (1960); *Phil. Mag.*, **42**, 441 (1951).
(23) W. Kanzig and M. H. Cohen, *Phys. Rev. Lett.*, **3**, 509 (1959); H. R. Zeller and W. Kanzig, *Helv. Phys. Acta*, **40**, 845 (1967); H. R. Zeller, R. T. Shuey, and W. Kanzig, *J. Phys. (Paris), Suppl.*, **28**, C4 (1967).
(24) J. E. Wertz and J. R. Bolton, "Electron Spin Resonance," McGraw-Hill, New York, N. Y., 1972, Chapters 11 and 12.
(25) E. Ishiguro and M. Kobori, *J. Phys. Soc. Jap.*, **22**, 266 (1967).
(26) F. J. Adrian, E. L. Cochran, and V. A. Bowers, *J. Chem. Phys.*, **59**, 56 (1973).
(27) D. M. Lindsay, D. R. Herschbach, and A. L. Kwiram, *Chem. Phys. Lett.*, **25**, 175 (1974).
(28) J. A. Ibers and W. C. Hamilton, *J. Chem. Phys.*, **44**, 1748 (1966).
(29) J. N. Wilson, R. M. Curtis, and C. T. Goetschel, *J. Appl. Crystallogr.*, **4**, 260 (1971).
(30) A. R. Young, T. Hirata, and S. I. Morrow, *J. Amer. Chem. Soc.*, **86**, 20 (1964).
(31) C. P. Slichter, "Principles of Magnetic Resonance," Harper and Row, New York, N. Y., 1963, Chapter 3.
(32) J. Levy, *J. Phys. C.*, **2**, 1371 (1969); *Phys. Rev. B*, **1**, 4261 (1970); **2**, 232 (1970).